THE JOURNAL OF PHYSICAL CHEMISTRY B

Article

pubs.acs.org/JPCB

Ion Intensity and Thermal Proton Transfer in Ultraviolet Matrix-Assisted Laser Desorption/Ionization

I-Chung Lu,[†] Chuping Lee,[†,‡] Hui-Yuan Chen,[†] Hou-Yu Lin,[†,‡] Sheng-Wei Hung,[†] Yuri A. Dyakov,[†] Kuo-Tung Hsu,[§] Chih-Yu Liao,[§] Yin-Yu Lee,[§] Chien-Ming Tseng,[⊥] Yuan-Tseh Lee,[†,‡] and Chi-Kung Ni*[,†,∥]

[†]Institute of Atomic and Molecular Sciences, Academia Sinica, Taipei 10617, Taiwan

[‡]Department of Chemistry, National Taiwan University, Taipei 10617, Taiwan

[§]National Synchrotron Radiation Research Center, Hsinchu 30076, Taiwan

[⊥]Department of Applied Chemistry, National Chiao Tung University, Hsinchu 30010, Taiwan

[∥]Department of Chemistry, National Tsing Hua University, Hsinchu 30013, Taiwan

ABSTRACT: The ionization mechanism of ultraviolet matrix-assisted laser desorption/ionization (UV-MALDI) was investigated by measuring the total cation intensity (not including sodiated and potasiated ions) as a function of analyte concentration (arginine, histidine, and glycine) in a matrix of 2,4,6-trihydroxyacetophenone (THAP). The total ion intensity increased up to 55 times near the laser fluence threshold as the arginine concentration increased from 0% to 1%. The increases were small for histidine, and a minimal increase occurred for glycine. Time-resolved fluorescence intensity was employed to investigate how analytes affected the energy pooling of the matrix. No detectable energy pooling was observed for pure THAP and THAP/analyte mixtures. The results can be described by using a thermal proton transfer model, which suggested that thermally induced proton transfer is crucial in the primary ion generation in UV-MALDI.

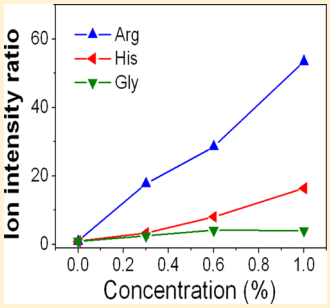

INTRODUCTION

Since being introduced by Tanaka,[1] Karas, and Hillenkam,[2] matrix-assisted laser desorption/ionization (MALDI) has become one of the most widely used techniques for performing mass analysis of biomolecules. In MALDI, analytes are mixed with a suitable matrix and then placed onto a sample holder. Ultraviolet (UV) laser pulses strike the target, releasing numerous analyte and matrix molecules. The desorbed molecules include ions and neutrals. The ions are subsequently analyzed using a mass spectrometer. Unfortunately, no single matrix is suitable for all analytes. Although using the appropriate matrix is a crucial parameter for successful MALDI mass analysis, selecting a matrix remains a trial and error process because the ionization mechanism of MALDI remains unclear.

Generating the first ions remains the most controversial part of the ionization mechanism. Several mechanisms have been proposed to explain the ion generation mechanism in MALDI, including direct multiphoton ionization,[3,4] the lucky survivor model,[5] thermal ionization of photoexcited matrices,[6] the energy pooling model,[7,8] excited state proton transfer,[9] the polar fluid model,[10,11] thermal reactions on solid state surfaces,[12] and the thermal proton transfer model.[13] However, the effects of each mechanism in MALDI are difficult to determine because it is not easy to quantitatively measure the contributions of these mechanisms.

Among the various mechanisms, only the thermal ionization of the photoexcited matrix model, the energy pooling model, thermal reactions on solid state surfaces, and the thermal proton transfer model can be quantitatively described. In the thermal proton transfer model, the total ion generation efficiency changes when an analyte is added into the matrix. This is because analyte ions can be generated as primary ions in the proton transfer between the matrix and analyte, $M + A \rightarrow (M-H)^- + AH^+$, or as the secondary ions in ion−molecule reactions in the thermal proton transfer model. When an analyte is added to the matrix, the thermal proton transfer model predicts that the total number of ions can substantially increase if the proton transfer efficiency between matrix and analyte is larger compared with the proton transfer efficiency between matrix molecules. By contrast, in the thermal ionization of photoexcited matrix and energy pooling models, the matrix ions are the primary ions, and the analyte ions are the secondary ions generated from ion−molecule reactions between the matrix ions and neutral analytes. When an analyte is added to the matrix, the thermal ionization of the photoexcited matrix and energy pooling models predicts that the total number of ions remains constant if the photoexcited matrix or the energy pooling of the matrix is not affected by the analyte.

This study presents two types of experiments. First, analytes that exhibited distinct proton affinities were separately added to

Received: January 23, 2014
Revised: March 24, 2014
Published: March 25, 2014

   dx.doi.org/10.1021/jp5008076 | J. Phys. Chem. B 2014, 118, 4132−4139

the matrix, and the total cation intensity was measured as a function of the analyte concentration. With regard to analytes that exhibit large proton affinities, we demonstrated that the total cation intensity increased as the analyte concentration increased. By contrast, regarding analytes that exhibit small proton affinities, the total cation intensity remained constant. Second, we investigated how analytes affected the energy pooling of the matrix by using time-resolved fluorescence. A previous study[14] showed that the energy pooling of the trihydroxyacetophenone (THAP) matrix was too small to be detected. Energy pooling does not likely play an essential role in the ion generation of MALDI in the THAP matrix. In this work, we demonstrated that the analytes used in this study did not affect the energy pooling properties of THAP, and no energy pooling was observed in the THAP/analyte mixtures. A quantitative description of the thermal proton transfer model is provided to demonstrate that the increase of total ion intensity can be described using the thermal proton transfer model.

EXPERIMENTAL METHODS

Ion Intensity. The cation intensities of MALDI were measured using a commercial time-of-flight mass spectrometer (Autoflex III, Bruker Daltonik). The matrix used in this study was 2,4,6- trihydroxyacetophenone (THAP 98%). The analytes, arginine (Arg), histidine (His), and glycine (Gly), were purchased from Sigma-Aldrich and used without further purification. The matrix and analytes were separately ground into fine powder. The samples were prepared by mixing the matrix and analyte powders in a proper molar ratio. The powder mixture was placed in microtubes, which were shaken using a mixer (Uzusio, VTX-3000L, Japan) for 1 h and subsequently pressed using a Teflon rod to form thin disks approximately 0.5−1 mm thick. The thin disks were affixed to the stainless steel sample plate by using a thin film of commercially available solid adhesive (UHU Stic, UHU GmbH & Co. KG, Germany). This sample preparation method yielded a homogeneous analyte distribution throughout the sample area and has been previously used to conduct quantitative analyses in MALDI.[15,16] A laser beam set at 355 nm from the third harmonic of a built-in Nd:YAG laser (pulse duration of 7 ns) was used in this experiment. The laser spot size was 300 μm in diameter on the sample surface.

Time-Resolved Fluorescence. To investigate how the analytes affected the energy pooling of the matrix, the time-resolved fluorescence intensity was measured using the third harmonic of a Nd:YAG laser (355 nm, < 20 ps pulse duration, model no. PL2210D-1K-P20, Ekspla, Lithuania) to excite solid samples in a vacuum (1×10^{-6} Torr), and a streak camera (1 ps time resolution, no. C10910-S21, Hamamatsu Photonics K. K., Japan) was used to detect fluorescence. Time-resolved fluorescence measurements were described in a previous report.[14] The sample preparation method used was the same as that used to measure the ion intensity.

RESULTS

The ratio of the total cation intensity presented in this study was defined as the total cation intensity per laser shot of the mixed matrix and analyte samples divided by the total cation intensity per laser shot of the pure matrix sample at the same laser fluence. Only protonated THAP and protonated analytes were considered. Because the generation of metal ions is not related to the proton transfer, ions related to metal cations, such as Na^+, K^+, sodiated ions, and potasiated ions, were not considered. The ratios of negative ions were not measured because we could not distinguish whether the counterions of these negative ions were protonated or metal-related cations, and only the ratios of cations are reported herein.

Figures 1a and 2a show the ratios of total cation intensity as a function of the analyte concentrations of various amino acids in

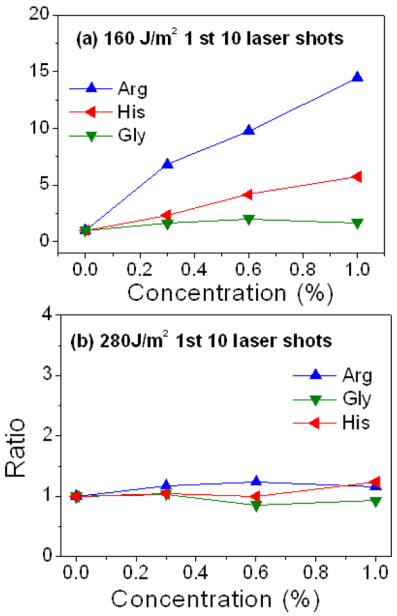

Figure 1. Ratio of total ion intensity of the first 10 laser shots as a function of analyte concentration for various amino acids in THAP.

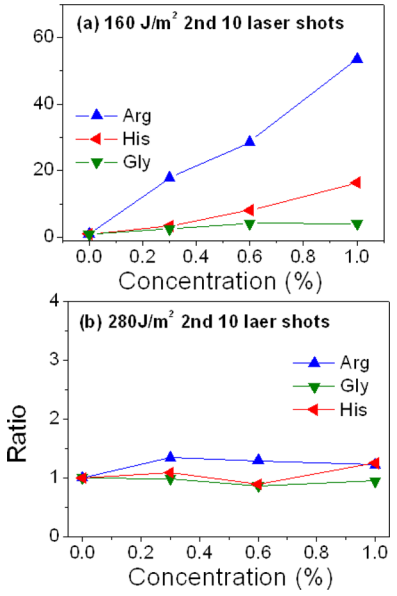

Figure 2. Ratio of total ion intensity of the second 10 laser shots as a function of analyte concentration for various amino acids in THAP.

THAP. The laser fluence was 160 J/m^2, which was near the threshold of MALDI for THAP. The ratios increased as the Arg concentration increased. The total ion intensity of 1% of Arg in THAP was 15 times larger than that of the pure THAP sample regarding the first set of 10 laser shots at the same sample position. It increased by 55 times in the second set of 10 laser shots at the same sample position. When the analyte was

dx.doi.org/10.1021/jp5008076 | J. Phys. Chem. B 2014, 118, 4132−4139

changed from Arg to His, the increase in the total cation intensity diminished. Almost no change was observed in the total cation intensity of the Gly/THAP mixture. Figures 1b and 2b show that the increases of the total cation intensity ratios were small for all analytes at high laser fluence levels.

Each data point in Figures 1 and 2 represents the average intensity per laser shot of 10 samples, and 20−80 mass spectra were taken from each sample, representing 20−80 randomly chosen distinct laser striking positions. For each position, the mass spectra of the first and second sets of 10 laser shots were separately accumulated. The number of mass spectra (200−800) depended on the analyte concentration and laser fluence. Regarding pure THAP at low laser fluence levels, 800 mass spectra were recorded because the ion intensity in most of the mass spectra was zero. However, only 200 mass spectra were recorded for 1% Arg in THAP at high laser fluence because large ion intensities were observed in each mass spectrum. The ion intensities were divided into several regions, and the mass spectra were sorted according to the ion intensity. Figure 3

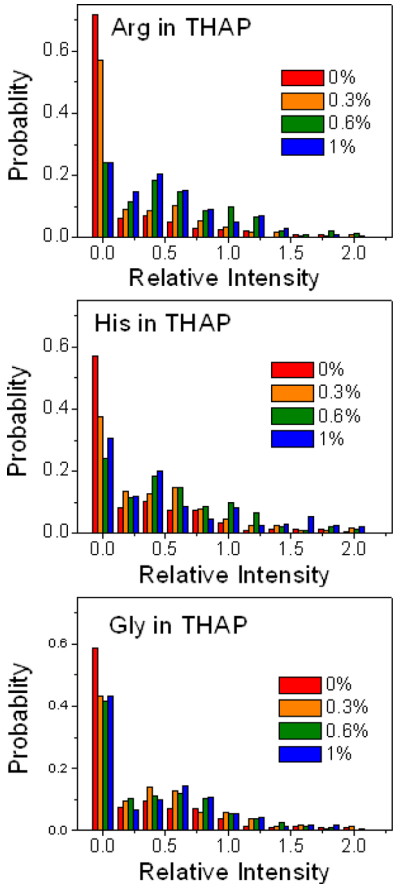

Figure 3. Probability of ion intensity distribution of the first 10 laser shots at laser fluence 160 J/m^2 for different analytes.

shows the probabilities of ion intensity distribution, defined as the number of mass spectra in each ion intensity region divided by the total number of mass spectra. No ions were detected (i.e., the intensity was zero) in most of the pure THAP spectra. However, the probability of zero ion intensity substantially decreased when the Arg concentration increased. High Arg concentrations also greatly increased the probability of large ion intensity. Moreover, the distribution does not considerably change when various Gly concentrations are used.

We previously reported[14] that the S_1 lifetime of the pure THAP matrix does not change as laser fluence increases, indicating that no energy pooling occurs. The S_1 lifetime of the THAP in analyte/THAP mixtures also remained unchanged as laser fluence increases, as illustrated in Figure 4. These findings suggest that energy pooling still does not occur when analytes are added to THAP.

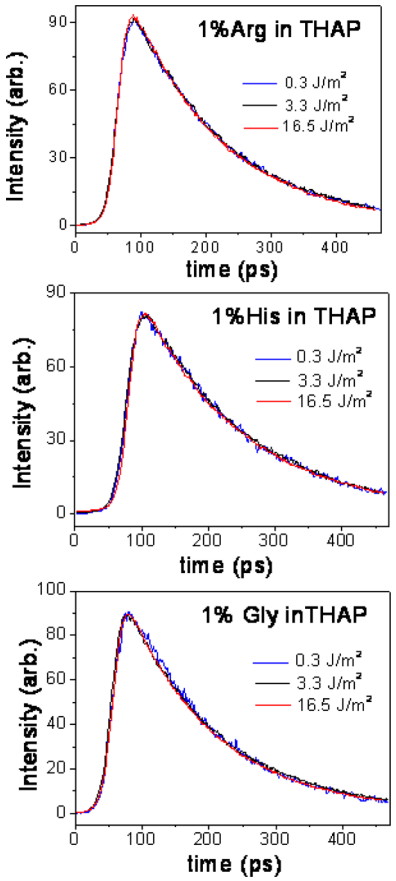

Figure 4. Time-resolved fluorescence intensity for analyte/THAP mixture at various laser fluences.

DISCUSSION

Effects of Analytes on Energy Pooling. S_1-S_1 annihilation (energy pooling) was suggested as a key step in primary ion generation in the energy pooling model.[7] In the energy pooling model, primary ions are generated from exciton−hopping followed by annihilation between two molecules in the first electronic excited singlet state, S_1-S_1, (energy pooling). The S_1-S_1 annihilation generates matrix molecules in the highly electronic excited singlet state, S_n. The subsequent annihilation between one molecule in the first electronic excited singlet state and the other in highly electronic excited singlet state (S_1-S_n energy pooling), or thermal ionization from S_n generates the first ions. The subsequent ion−molecule reactions between matrix ions and matrix neutrals or between matrix ions and analyte neutrals produce the ions observed in the mass spectra.

The fluorescence quantum yields of 2-aminobenzoic acid, 2,5-dihydroxybenzoic acid (2,5-DHB), and 3-hydroxypicolinic acid decrease as the laser fluence increases; this has been used as the evidence for S_1-S_1 annihilation.[17,18] In a previous

dx.doi.org/10.1021/jp5008076 | J. Phys. Chem. B 2014, 118, 4132−4139

report,[14] energy pooling was investigated by time-resolved fluorescence experiment using a short laser pulse (355 nm, 20 ps pulse width) for excitation and a streak camera (1 ps time resolution) for fluorescence detection. It provides a better method to investigate the S_1-S_1 annihilation.

We showed that the S_1 lifetime of 2,5-DHB decreased as the laser fluence increased.[14] These results confirmed that two molecules reacted in the S_1 state, and energy pooling was a possible reaction. The time-resolved fluorescence measurements also showed that no energy pooling was detected for THAP.[14] In the current study, we demonstrated that the results did not change when analytes were added into the THAP, as illustrated in Figure 4 by the invariable lifetimes at various laser fluences. This lack of lifetime change suggests that the total ion intensity ratio as a function of analyte concentration should remain the same if energy pooling is crucial in the generation of first ions in MALDI. This contradicts the experimental observations.

Thermal Proton Transfer Model. We discovered that the changes of the total ion intensity ratios of various amino acids and concentrations can be described by using the thermal proton transfer model.[13] In the thermal proton transfer model, the ions generated in MALDI were primarily yielded by thermally induced reactions at high temperatures. Proton transfer exhibits the smallest heat of reaction, which is readily enhanced by high temperatures. When the temperature increases and the solid sample turns into liquid, these reactions reach equilibrium because of the low barrier height of proton transfer reactions and high collision frequency between molecules in liquid. During desorption, the ion intensities of various species may change because of reactions in the gas plume. Some reactions reach equilibrium in the gas phase, whereas others do not. For example, ion generations from proton transfer reactions and the ion−ion recombination ($M + M \leftrightarrows (MH)^+ + (M - H)^-$ and $M + A \leftrightarrows (AH)^+ + (M - H)^-$) do not reach equilibrium in the gas phase because of the high heat of reactions in the gas phase in forward reactions, the low concentration of ions in backward reactions, and the rapid expansion of gas plume in vacuum. The total ion-to-neutral ratio in the gas phase remains similar to the ratio in the liquid phase. However, the ion−molecule reaction, $(MH)^+ + A \leftrightarrows M + (AH)^+$, may reach equilibrium in the gas phase because of the low reaction barrier height and high concentrations of analyte and matrix neutrals. The ion concentrations of each species change because of the ion−molecule reactions in the gas phase, but the total ion intensity does not change from the liquid phase to the gas phase. Detailed numerical calculations were provided in our previous report.[13]

In this study, we focused on total ion intensity. The total ion intensity increases as the analyte concentration increases simply because the proton transfer reaction $A + M \leftrightarrows AH^+ + (M - H)^-$ shifts from reactants (neutral) to products (ions) due to the increase of analyte concentration. The shift is large for analytes with large proton affinities. In the following paragraphs, equations were derived to illustrate how thermal proton transfer can describe the experimental data.

Formulation of Total Ion Intensity Ratio. The thermally induced reactions in liquid phase include the proton disproportionation between the matrix M, proton disproportionation between the matrix and analyte A, and proton transfer reaction between the protonated matrix and analyte.

$$M_{(l)} + M_{(l)} \leftrightarrows MH^+_{(l)} + (M - H)^-_{(l)} \quad (1)$$

$$A_{(l)} + M_{(l)} \leftrightarrows AH^+_{(l)} + (M - H)^-_{(l)} \quad (2)$$

$$MH^+_{(l)} + A_{(l)} \leftrightarrows M_{(l)} + AH^+_{(l)} \quad (3)$$

where subscript letter l represents the liquid phase If the deprotonation energy of the analyte is sufficiently small, the following proton disproportionation reactions also occur:

$$A + M \leftrightarrows (A - H)^- + (M + H)^+ \quad (4)$$

$$A + A \leftrightarrows (A - H)^- + (A + H)^+ \quad (5)$$

$$A + (M - H)^- \leftrightarrows (A - H)^- + M \quad (6)$$

The corresponding Gibbs free energy and equilibrium constants of these reactions are ΔG_1, ΔG_2, ΔG_3, ΔG_4, ΔG_5, ΔG_6, K_1, K_2, K_3, K_4, K_5, and K_6. The initial concentrations of the matrix, analytes, and ions are m, a, and zero, respectively. At equilibrium, the concentrations of M, A, $(M\text{-}H)^-$; MH^+; AH^+; and $(A - H)^-$ are $m - x - y$; $a - z - w$; x, y, z; and w, respectively. At equilibrium, the following equations are yielded:

$$K_1 = \frac{xy}{(m - x - y)^2} \quad (7)$$

$$K_2 = \frac{xz}{(m - x - y)(a - z - w)} \quad (8)$$

$$K_3 = \frac{(m - x - y)z}{(a - z - w)y} \quad (9)$$

$$K_4 = \frac{wy}{(a - z - w)(m - x - y)} \quad (10)$$

$$K_5 = \frac{wz}{(a - z - w)^2} \quad (11)$$

$$K_6 = \frac{w(m - x - y)}{(a - z - w)x} \quad (12)$$

On the basis of the charge balance, the following is derived:

$$x + w = y + z \quad (13)$$

Reactions 1−6 are not independent. For example, the sum of reactions 1 and 3 equals to reaction 2, and K_1, K_2, and K_3 are related as follows:

$$K_1K_3 = K_2 \quad (14)$$

The other relationships can be described as follows:

$$K_3K_4 = K_5 \quad (15)$$

$$K_1K_6 = K_4 \quad (16)$$

Because ion concentrations are much smaller compared with neutral concentrations,[19] $m - x - y \approx m$ and $a - z - w \approx a$ are adequate approximations. Using these approximations and eqs 7−16 yields the following:

$$[M - H]^- = x = m\sqrt{K_1\frac{\left(1 + \frac{a}{m}K_3\right)}{\left(1 + \frac{a}{m}K_6\right)}} \quad (17)$$

dx.doi.org/10.1021/jp5008076 | J. Phys. Chem. B 2014, 118, 4132−4139

$$[M + H]^+ = y = m\sqrt{K_1\frac{\left(1 + \frac{a}{m}K_6\right)}{\left(1 + \frac{a}{m}K_3\right)}} \quad (18)$$

$$[A + H]^+ = z = aK_3\sqrt{K_1\frac{\left(1 + \frac{a}{m}K_6\right)}{\left(1 + \frac{a}{m}K_3\right)}} \quad (19)$$

$$[A - H]^- = w = aK_4\sqrt{\frac{1}{K_1}\frac{\left(1 + \frac{a}{m}K_3\right)}{\left(1 + \frac{a}{m}K_6\right)}} \quad (20)$$

The ratio of total positive ions as a function of analyte concentration can be calculated using eqs 18 and 19.

$$\gamma = \frac{\text{Cations from mixture}}{\text{Cations from pure matrix}} = \frac{[M + H]^+ + [A + H]^+}{[M + H]^+} = \sqrt{1 + \frac{a}{m}K_3} \times \sqrt{1 + \frac{a}{m}K_6} = \sqrt{1 + \frac{a}{m} \times e^{-\Delta G_3/RT}} \times \sqrt{1 + \frac{a}{m} \times e^{-\Delta G_6/RT}} \quad (21)$$

T represents the temperature before desorption occurs. Identical results for the ratio of negative ions can be obtained using eqs 17 and 20.

Because a/m and equilibrium constants are positive, the ratio γ always increases as the analyte concentration increases. Ratios of various concentrations can be easily compared if the temperature, which depends on the absorption cross section and heat capacity, remains the same. Because the analytes exhibit distinct absorption cross sections and heat capacities compared with the matrix, constant temperature is a good approximation if the amount of analyte in the matrix remains small. We maintained the analyte concentration below 1% to ensure the absorption cross section and heat capacity of matrix/analyte mixtures were not substantially different from the values of pure matrix. For a given matrix at a given temperature, the ratio of ions increase is large and can be easily measured if $a/m \times K_3$ or $a/m \times K_6$ is substantially larger than 1. This occurs when a/m is not extremely small and the proton affinity (or basicity) of the analyte is substantially larger than that of the matrix (large K_3) or the deprotonation energy of the analyte is much smaller than that of the matrix (large K_6). Equation 21 also shows that the increase of the ratio is large when the temperature is low; this occurs when the laser fluence is small.

Estimation of Ion Intensity Ratio. The ratio of total ion intensity can be estimated if the temperature before desorption and Gibbs free energy in eq 21 are known. Details regarding the temperature and Gibbs free energy calculations were reported in a previous work.[13] Only a brief description is provided herein.

The relation between laser fluence and the temperature of a sample before desorption occurs can be described by the heat equation assuming that desorption is absent during the laser pulse duration and thermal energy is confined within the laser irradiated volume, as follows:

$$F \equiv \int_{t_i}^{t_f} I dt = \frac{\rho_0}{\alpha(1 - \Phi)} \int_{T_0}^{T} c_p(T) dT + \Delta m(F) \times L \quad (22)$$

where ρ_0, c_p, α, Φ, I, Δm, and L denote the mass density before laser irradiation, specific heat capacity, absorption cross section, fluorescence quantum yield of the matrix, laser intensity, molecular desorption per unit area, and latent heat of fusion, respectively; and T_0, F, and t_i, and t_f represent the initial temperature, laser fluence, and the start and stop times of the laser pulse, respectively. The temperature-dependent heat capacity can be calculated based on the molar heat capacity of the solid matrix by using a modified Einstein model, as follows:

$$C_v = 3R \times \left(\frac{h\nu}{kT}\right)^2 \times \frac{e^{h\nu/kT}}{(1 - e^{h\nu/kT})^2} + \frac{3}{2}R + \sum_{i}^{3N-6-m} R \times \left(\frac{h\nu_i}{kT}\right)^2 \times \frac{e^{h\nu_i/kT}}{(1 - e^{h\nu_i/kT})^2} \quad (23)$$

where h is the Planck constant, k is the Boltzmann constant, ν is the oscillator frequency between molecules, and ν_i is the vibrational frequency of the matrix. The specific heat capacity was determined based on the relation between the specific and molar heat capacities, $C_p = C_p/M_w$ and $C_p = C_v + VT(a^2/b)$, where a is the coefficient of thermal expansion and b is the isothermal compressibility. We did not have absorption cross section of solid THAP at 355 nm. An estimated value (10^5 cm^{-1}) similar to the absorption cross sections of matrices 2,5-dihydroxybenzoic acid (2,5-DHB), sinapinic acid (SA), and ferulic acid (FA) at 355 nm[20] was used in this study.

The Gibbs free energy of reaction 3 can be calculated on the basis of the summation of the Gibbs free energies of the following three reactions.

$$MH^+_{(l)} + A_{(l)} \rightarrow MH^+_{(g)} + A_{(g)} \quad (24)$$

$$MH^+_{(g)} + A_{(g)} \rightarrow M_g + AH^+_{(g)} \quad (25)$$

$$M_g + AH^+_{(g)} \rightarrow M_{(l)} + AH^+_{(l)} \quad (26)$$

where subscript g represents the gas phase. Reaction 25 represents the proton transfer reaction in the gas phase. Reaction 24 is the reverse reaction of solvation, and reaction 26 is the reaction of solvation. Equations 24 and 26 include the solvation energy of both neutrals and ions.

Table 1 lists the proton affinities and deprotonation energies of analytes and THAP in the gas phase as obtained from literature[21−24] and ab initio calculations (Gaussian 09).[25,26] The calculated values of proton affinities and deprotonation energies depend on the positions of the protons detached from the molecule. We listed only the largest proton affinity and smallest deprotonation energy of each molecule. Among these analyte molecules, Arg exhibited the largest proton affinity and Gly and THAP exhibited the smallest proton affinity. The deprotonation energy of THAP was smaller compared with that of the analytes used in this study. The Gibbs free energy of reaction 25 was obtained using the approximation $\Delta G_{25} = \Delta H_{25}$.

The solvation energies of both neutrals and ions were obtained using the polarizable continuum model (PCM)[27]

Table 1. Heats of Reaction (kJ/mol) in the Gas Phase from Ab Initio Calculations and Previous Reports[a]

	$X + H^+ \rightarrow XH^+$	$X \rightarrow (X - H)^- + H^+$
	ΔH	ΔH
THAP	−887.8, −882,[21] −893[22]	1371.1
arginine	−990.2, −1016,[23] −1025[24]	1415.0
histidine	−973, −955,[23] −969[24]	1408.7
glycine	−883.6, −885,[23] −859.9[23]	1424.2

[a]Superscripts denote the references.

dx.doi.org/10.1021/jp5008076 | J. Phys. Chem. B 2014, 118, 4132−4139

included in the Gaussian 09 computational package. To determine the solvation energy, the dielectric constant of polar liquids (e.g., THAP), ε, was calculated as a function of temperature by using the Kirkwood−Frohlich equation:[28]

$$g\mu^2 = \frac{9kT}{4\pi\rho_N}\frac{(\varepsilon - \varepsilon_\infty)(2\varepsilon + \varepsilon_\infty)}{\varepsilon(\varepsilon_\infty + 2)^2} \quad (27)$$

and Clausius−Mossotti equation:

$$\frac{\varepsilon_\infty - 1}{\varepsilon_\infty + 2} = \frac{4\pi}{3}\alpha'\rho_N \quad (28)$$

The approximation $g = 1$ was used in the calculations because only the high temperature region was relevant to this study. The polarizability and dipole moment (calculated using the Gaussian 09 MP2/6-31+G** method) for THAP were $\alpha' = 1.43 \times 10^{-23}$ cm^3 and $\mu = 6.6$ D, respectively. The computed polarizability value includes the electronic and vibrational polarizabilities. The density as a function of temperature in eqs 27 and 28 was calculated as follows:

$$\rho_N(T) = \frac{\rho_N(T = 300K)}{(1 + 0.0008 \times \Delta T)} \quad (29)$$

where the room temperature density was derived on the basis of the experimental measurements,[29] and the coefficient of the volumetric thermal expansion, 8×10^{-4} (K^{-1}), was derived on the basis of the average volumetric expansion coefficient of common liquids.[30] A similar method was used to obtain the approximation of ΔG_6, and Table 2 lists the ΔG_3 and ΔG_6 of

Table 2. Calculated Gibbs Free Energy (kJ/mol) of Reaction 3 and 6 in Liquid THAP and Theoretical Prediction of Total Ion Intensity Ratio for 1% Analyte

temp (K)	900			1250		
	ΔG_3	ΔG_6	ratio	ΔG_3	ΔG_6	ratio
arginine	−129	23	554	−124	26	38
histidine	−85	43	29	−84	42	5
glycine	−56	−2	4	−48	4	1

the analytes. The solvation energies of reactants and products (reactions 24 and 26) approximately cancel each other. The Gibbs free energies in the liquid phase were dominated by the heat of the reactions in the gas phase.

The first term on the right of eq 21, $(1 + (a/m) \times e^{-\Delta G_3/RT})^{1/2}$, is substantially larger than 1 for Arg and close to 1 for Gly. The deprotonation energies of the analytes were all larger compared with that of THAP. Therefore, the second term on the right of eq 21,$(1 + (a/m) \times e^{-\Delta G_6/RT})^{1/2}$, is close to 1 for all analytes. Table 2 lists the theoretical predictions of total ion intensity ratios. Regarding 1% Arg in THAP (a/m = 1%), the ratios of eq 21 for temperatures at 900 K (180/m^2) and 1200 K (280/m^2) are approximately 554 and 38, respectively. The ratio is large because Arg has a larger proton affinity than THAP does. These ratios become 29 and 5 for 1% His in THAP. By contrast, the ratios of 1% Gly in THAP always remain close to 1 at these temperatures because of the small proton affinity and large deprotonation energy of Gly. For a given analyte, Table 2 also shows that the ion intensity ratio is small when the temperature is high. According to eq 21, the ion intensity ratio is close to 1 if the temperature is very high.

The predictions obtained using the thermal proton transfer model show the same trend as the experimental measurements (i.e., the ion intensity ratio is large for analytes of large proton affinity and it is small at high laser fluence). However, the ion intensity ratios in the theoretical calculations were typically larger than those from the experimental measurements. In addition to the uncertainties in calculations (e.g., temperature and dielectric constant), one possible explanation of large ion intensity ratios from calculations is the overestimated analyte-to-matrix molar ratio (a/m) in calculations. The MALDI samples used in this study were prepared by mixing matrix and analyte powders. These powders were small particles exhibiting a diameter of approximately 10−50 μm. The analyte and matrix molecules were separately confined within these particles and were not mixed homogeneously at the molecular level. Because only the analyte molecules on the surface of the analyte powder directly contacted the matrix powder, not all analyte molecules were dissolved into the hot matrix liquid when laser irradiation increased the temperature of the matrix powder. Therefore, the actual molar ratio between the matrix and analyte was substantially smaller compared with the molar ratio calculated on the basis of the entire powder sample. As a result, the ion intensity ratios predicted as a result of the calculations were larger than those yielded by the experimental measurements. According to eq 21, the overestimated molar ratio has substantial effects in analytes that exhibits large proton affinities but causes almost no effect in analytes that exhibit small proton affinities.

In principle, using the dried droplet method to prepare samples provides the possibility of mixing the matrix and analyte molecules at the molecular level. However, as the solvent evaporates from the droplet, the drying process typically begins at the edge of the droplet and ends at the center of the droplet. Because of the different solubilities of the matrix and analytes in a solvent, the molar ratios of the matrix to analyte of the dried sample change between the sample edge and center. The sizes and shapes of the crystals produced at the edge of dried droplets differ from those produced at the center. Consequently, samples prepared using the dried droplet method are highly inhomogeneous in molar ratio and also in crystal size and shape; therefore, they were not suitable for use in this study.

The overestimated molar ratio (a/m) in calculations can be confirmed on the basis of the increase of the total ion intensity ratio of the second set of 10 laser shots. As shown in Figures 1 and 2, the total ion intensity ratio of the second set of 10 laser shots was much larger than that of the first set of 10 laser shots, and the ratio was substantially closer to theoretically predicted values. This is because the residual heat of the previous laser shots melted sections of the matrix particles, improving the mixture of the matrix and analyte. As a result, the difference of molar ratios (a/m) between the second set of 10 laser shots and calculations was smaller compared with the difference of molar ratios (a/m) between the first set of 10 laser shots and calculations.

Comparison to the Mechanism Proposed by Kim et al. Kim et al. reported that the abundance of each ion in a (MALDI) spectrum looked thermally determined.[31−33] We would like to make a simple comparison of our model and the ionization mechanism proposed by Kim et al. Two major differences were found between our model and Kim's mechanism. First, Kim et al. proposed that analyte ions, AH^+, can be generated only from reaction 3 and that no conclusive mechanism is responsible for the primary ion (MH^+) formation. Our model suggests that analyte ions are not only

dx.doi.org/10.1021/jp5008076 | J. Phys. Chem. B 2014, 118, 4132−4139

generated from reaction 3 but also from reaction 2. Reactions 1, 2, 4, and 5 are responsible for the primary ion generation. Second, Kim et al. found that the total ion intensity did not change with analyte concentration. The analyte-to-matrix molar ratios of solid samples in their experiments ranged from 0% to 0.1%, and laser fluence was 2−10 times of the threshold. Their analyte concentration was much smaller than the concentration we used in this work, and laser fluence was much larger than the laser fluence we used in this work. According to eq 21, our model predicts that the increase of total ion intensity is small when the concentration of analyte is small and/or laser fluence is large. Equation 21 can explain why the ion intensity does not change with analyte concentration and laser fluence in Kim's experiment. On the other hand, we demonstrated that the total ion intensity increased significantly at high analyte concentration and low laser fluence. This observation cannot be explained by the mechanism proposed by Kim et al.

■ CONCLUSION

In contrast to the thermal ionization of the photoexcited matrix and energy pooling models, in which matrix ions must first be generated to initiate proton or charge transfers between matrix ions and neutral analytes, the thermal proton transfer model suggests that analyte ions can be directly generated from the thermal proton transfer reaction between the matrix and the analyte. Because the analytes used in this work did not affect the energy pooling rate, the energy pooling model cannot explain why the total ion intensity increased as the analyte concentration increased. However, we demonstrated that the increase can be explained by using the thermal proton transfer model. Because most peptides and proteins exhibit proton affinities that are both larger than the proton affinities of the matrix used in this study and larger than the common matrices used in UV-MALDI, thermal proton transfer reactions must play an essential role in UV-MALDI processes.

■ AUTHOR INFORMATION

Corresponding Author

*E-mail: ckni@po.iams.sinica.edu.tw. Tel.: 886-223668277.

Notes

The authors declare no competing financial interest.

■ ACKNOWLEDGMENTS

We acknowledge the support by Thematic Research Program, Academia Sinica, Taiwan (AS-102-TP-A08) and National Science Council, Taiwan (NSC 100-2113-M-001-026-MY3).

■ REFERENCES

(1) Tanaka, K.; Waki, H.; Ido, Y.; Akita, S.; Yoshida, Y. Protein and Polymer Analyses up to m/z = 100 000 by Laser Ionization Time-of-Flight Mass Spectrometry. *Rapid Commun. Mass Spectrom.* **1988**, *2*, 151−153.

(2) Karas, M.; Hillenkamp, F. Laser Desorption Ionization of Proteins with Molecular Masses Exceeding 10 000 Da. *Anal. Chem.* **1988**, *60*, 2299−2301.

(3) Karas, M.; Bachmann, D.; Bahr, U.; Hillenkamp, F. Matrix-Assisted Ultraviolet-Laser Desorption of Nonvolatile Compounds. *Int. J. Mass Spectrom. Ion Processes* **1987**, *78*, 53−68.

(4) Ehring, H.; Karas, M.; Hillenkamp, F. Role of Photoionization and Photochemistry in Ionization Progress of Organic-Molecules and Relevance for Matrix-Assisted Laser Desorption Ionization Mass Spectrometry. *Org. Mass Spectrom.* **1992**, *27*, 472−480.

(5) Karas, M.; Gluckmann, M.; Schafer, J. Ionization in Matrix-Assisted Laser Desorption/Ionization: Singly Charged Molecular Ions Are the Lucky Survivors. *J. Mass Spectrom.* **2000**, *35*, 1−12.

(6) Allwood, D. A.; Dyer, P. E.; Dreyfus, R. W. Ionization Modeling of Matrix Molecules in Ultraviolet Matrix-Assisted Laser Desorption/Ionization. *Rapid Commun. Mass Spectrom.* **1997**, *11*, 499−503.

(7) Knochenmuss, R. A Quantitative Model of Ultraviolet Matrix-Assisted Laser Desorption/Ionization. *J. Mass Spectrom.* **2002**, *37*, 867−877.

(8) Knochenmuss, R. A Quantitative Model of Ultraviolet Matrix-Assisted Laser Desorption/Ionization Including Analyte Ion Generation. *Anal. Chem.* **2003**, *75*, 2199−2207.

(9) Ludemann, H. C.; Hillenkamp, F.; Redmond, R. W. Photoinduced Hydrogen Atom Transfer in Salicylic Acid Derivatives Used as Matrix-Assisted Laser Desorption/Ionization (MALDI) Matrices. *J. Phys. Chem. A* **2000**, *104*, 3884−3893.

(10) Chen, X.; Carroll, J. A.; Beavis, R. C. Near-Uultraviolet-Induced Matrix-Assisted Laser Desorption/Ionization as a Function of Wavelength. *J. Am. Soc. Mass Spectrom.* **1998**, *9*, 885−891.

(11) Niu, S.; Zhang, W.; Chait, B. T. Direct Comparison of Infrared and Ultraviolet Wavelength Matrix-Assisted Laser Desorption/Ionization Mass Spectrometry of Proteins. *J. Am. Soc. Mass Spectrom.* **1998**, *9*, 1−7.

(12) Lai, Y. H.; Wang, C. C.; Lin, S. H.; Lee, Y. T.; Wang, Y. S. Solid-Phase Thermodynamic Interpretation of Ion Desorption in Matrix-Assisted Laser Desorption/Ionization. *J. Phys. Chem. B.* **2010**, *114*, 13847−13852.

(13) Chu, K. Y.; Lee, S.; Tsai, M. T.; Lu, I. C.; Dyakov, Y. A.; Lai, Y. H.; Lee, Y. T.; Ni, C. K. Thermal Proton Transfer Reactions in Ultraviolet Matrix-Assisted Laser Desorption/Ionization. *J. Am. Soc. Mass Spectrom.* **2014**, *25*, 310−318.

(14) Lin, H. Y.; Song, B.; Lu, I. C.; Hsu, K. T.; Liao, C. Y.; Lee, Y. Y.; Tseng, C. M.; Lee, Y. T.; Ni, C. K. Is Energy Pooling Necessary in UV-MALDI? *Rapid Commun. Mass Spectrom.* **2014**, *28*, 77−82.

(15) Kinsel, G. R.; Yao, D.; Yassin, F. H.; Marynick, D. S. Equilibrium Conditions in Laser-Desorbed Plumes: Thermodynamic Properties of Alpha-Cyano-4-Hydroxycinnamic Acid and Protonation of Amino Acids. *Eur. J. Mass Spectrom.* **2006**, *12*, 359−367.

(16) Land, C. M.; Kinsel, G. R. The Mechanism of Matrix to Analyte Proton Transfer in Clusters of 2,5-Dihydroxybenzoic Acid and the Tripeptide VPL. *J. Am. Soc. Mass Spectrom.* **2001**, *12*, 726−731.

(17) Ehring, H.; Sundqvist, B. U. R. Studies of the MALDI Process by Luminescence Spectroscopy. *J. Mass Spectrom.* **1995**, *30*, 1303−1310.

(18) Ludemann, H. C.; Redmond, R. W.; Hillenkamp, F. Singlet−Singlet Annihilation in Ultraviolet Matrix-Assisted Laser Desorption/Ionization Studied by Fluorescence Spectroscopy. *Rapid Commun. Mass Spectrom.* **2002**, *16*, 1287−1294.

(19) Tsai1, M. T.; Lee, S.; Lu, I. C.; Chu, K. Y.; Liang, C. W.; Lee, C. H.; Lee, Y. T.; Ni, C. K. Ion-to-Neutral Ratio of 2,5-Dihydroxybenzoic Acid in Matrix-Assisted Laser Desorption/Ionization. *Rapid Commun. Mass Spectrom.* **2013**, *27*, 955−963.

(20) Allwood, D. A.; Dreyfus, R. W.; Perera, I. K.; Dyer, P. E. UV Optical Absorption of Matrices Used for Matrix-Assisted Laser Desorption Ionization. *Rapid Commun. Mass Spectrom.* **1996**, *10*, 1575−1578.

(21) Breuker, K.; Knochenmuss, R.; Zenobi, R. Gas-Phase Basicities of Deprotonated Matrix-Assisted Laser Desorption/ionization Matrix Molecules. *Int. J. Mass Spectrom.* **1999**, *184*, 25−38.

(22) Mizra, S. P.; Raju, N. P.; Vairamani, M. Estimation of the Proton Affinity Values of Fifteen Matrix-Assisted Laser Desorption/Ionization Matrices Under Electrospray Ionization Conditions Using the Kinetic Method. *J. Am. Soc. Mass Spectrom.* **2004**, *15*, 431−435.

(23) Gorman, G. S.; Speir, J. P.; Turner, C. A.; Amster, I. J. Proton Affinities of the 20 Common Alpha-Amino-Acids. *J. Am. Chem. Soc.* **1992**, *114*, 3986−3988.

(24) Harrison, A. G. The Gas-Phase Basicities and Proton Affinities of Amino Acids and Peptides. *Mass Spectrom. Rev.* **1997**, *16*, 201−217.

(25) Frisch, M. J.; Trucks, G. W.; Schlegel, H. B.; Scuseria, G. E.; Robb, M. A.; Cheeseman, J. R.; Scalmani, G.; Barone, V.; Mennucci, B.; Petersson, G. A. et al.*Gaussian 09*, revision D.01; Gaussian, Inc.: Wallingford, CT, 2009.
(26) The geometries of the reactants and products were fully optimized using the hybrid density functional B3LYP method with the 6-31G* basis set. The energies of the reactants and products at B3LYP/6-31G* optimized geometries were calculated using the G3-type computational scheme, specifically the G3(MP2,CCSD)//B3LYP modification. Zero point energy (ZPE) corrections were taken into account by using B3LYP/6-31G* frequencies without scaling.
(27) Tomasi, J.; Mennucci, B.; Cammi, R. Quantum Mechanical Continuum Solvation Models. *Chem. Rev.* **2005**, *105*, 2999−3093.
(28) Frohlich, H. *Theory of Dielectrics*, 2nd ed.; Clarendon: Oxford, U. K., 1958.
(29) Mass density was measured from the volume change of saturated THAP aqueous solution by adding a given weght (1.1∼1.5 g) of THAP powder into the soltion.
(30) Volumetric Expansion Coefficients of Some Common Fluids, the Engineering Toolbox. http//www.EngineeringToolBox.com.
(31) Bae, Y. J; Shin, Y. S.; Moon, J. H.; Kim, M. S. Degree of Ionization in MALDI of Peptides: Thermal Explanation for the Gas-Phase Ion Formation. *J. Am. Soc. Mass Spectrom.* **2012**, *23*, 1326−1335.
(32) Ahn, S. H.; Park, K. M.; Bae, Y. J.; Kim, M. S. Quantitative Reproducibility of Mass Spectra in Matrix-Assisted Laser Desorption Ionization and Unraveling of the Mechanism for Gas-Phase Peptide Ion Formation. *J. Mass Spectrom.* **2013**, *48*, 299−305.
(33) Bae, Y. J.; Choe, J. C.; Moon, J. H.; Kim, M. S. Why do the Abundances of Ions Generated by MALDI Look Thermally Determined? *J. Am. Soc. Mass Spectrom.* **2013**, *24*, 1807−1815.